A Single-/Three-phase Compatible V2G Bidirectional On-Board Charger with Reconfigurable Structure

Yiu Pang Chan, Qingchun Li, Bhoopal Ponnuvelu, and River Tin-Ho Li,
Hong Kong Applied Science and Technology Research Institute Company Limited, Hong Kong SAR, China

***Abstract* -- a single-phase and three-phase grids compatible Vehicle-to-Grid (V2G) Electric Vehicle (EV) on-board bidirectional charger is proposed. The power stage and control method are configurated according to the grid voltage condition and charge/discharge command. An adaptive power control was derived to ensure minimum circulation loss of the DC/DC stage across the output voltage range. A liquid-cooled 11kW prototype of the proposed bidirectional charger was developed and experimentally verified. It achieved 96.5% maximum power conversion efficiency and 1.5kW/L power density. The proposed on-board V2G charger enables medium-speed EV charging at both single- and three-phase grids without the need for an off-board V2G charger.**

***Index Terms*—V2G, bidirectional charger, AC/DC converter, DAB converter.**

I. INTRODUCTION

Vehicle electrification has been taking place worldwide due to the benefits of effective reduction of greenhouse gas emissions and superior performance compared to fossil fuel vehicles [1]. According to Global EV Outlook 2021 [2], more than twenty countries have electrification targets or internal combustion engine bans for cars, and eight countries plus European Union have announced net-zero pledges. Hong Kong government decided to push for trials of electric public transport and commercial vehicles, as well as not to register fuel-powered private cars, including hybrids, by 2035 or earlier [3]. To facilitate EV adoption and popularity, increasing charging speed, improving changing flexibility, and upgrading grid infrastructure are necessary to cope with significant growth in the coming 5 to 10 years.

Nowadays, on-board chargers (OBCs) offer EVs the ability to charge directly from either single-phase or three-phase AC grids with unidirectional power transfer due to their convenience and simple hardware requirement. Typically, single-phase OBCs provide from 3.3kW to 6.6kW, and three-phase OBCs provide from 11kW to 22kW charging capabilities, respectively [4]. Compared with single-phase OBCs, the charging time of three-phase OBCs can be shortened by ~66% due to higher charger power. Different from the unidirectional type, bidirectional OBCs can support vehicle-to-grid (V2G) functionality by returning electrical energy to the grid, which can provide peak shaving function due to unstable renewable energy penetration or electricity cost saving due to time-variant electricity cost [5]. To make charging became highly flexible and convenient, an OBC with a reconfigurable structure, which can be single-phase and three-phase compatible with a bidirectional power flow control function, is proposed in this paper.

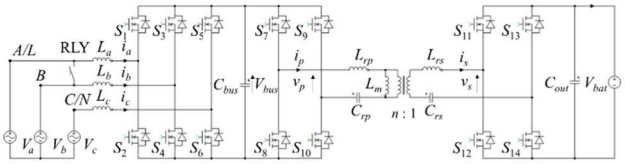

Fig. 1. Topology of the proposed V2G bidirectional OBC with reconfigurable structure

II. THE PROPOSED V2G BIDIRECTIONAL OBC DESIGN

The proposed OBC with a reconfigurable structure is a power conversion system which manages power flow from a single-phase AC grid terminal to a battery terminal, or vice versa, for energy storage applications, such as home power support. The proposed bidirectional charger is also compatible with a three-phase AC grid to boost the charging power to ~1.67 times the single-phase for a shorter charging time. The proposed V2G charger is a 2-stage structure; the topology and control method of the AC/DC stage can be switched between single-phase and three-phase according to the grid conditions. Fig. 1 shows the topology of the proposed V2G bidirectional OBC.

A. AC/DC stage design

The proposed OBC can automatically identify the AC grid connection between single-phase and three-phase and configure the topology and control accordingly. In single-phase AC grid condition, with connected nodes *L* and *N* to the input terminals of single-phase AC grid, respectively, and closed the relay between nodes *L* and *B*, the AC/DC stage is a 2-phase interleaved totem-pole topology with fixed frequency continuous conduction current mode control (CCM) for both battery charging and discharging operations. For single-phase totem-pole PFC modulation, MOSFETs S_1-S_4 operate at high switching frequency with the function as main boost switch and synchronous switch, while other MOSFETs S_5 and S_6 operate at line frequency as rectifier switches. During the positive half-line cycle, S_2 and S_4 are switching as a control switch with turn-on duty cycle D; S_1 and S_3 are switching as a synchronous switch, while S_5 is kept OFF and S_6 is kept ON. During the negative half-line cycle, S_1 and S_3 are switching as a

control switch with turn-on duty cycle D; S_2 and S_4 are switching as a synchronous switch, while S_5 is kept ON and S_6 is kept OFF. Like the boost converter, the output bus voltage of the single-phase totem-pole PFC converter can be calculated by $V_{bus} = \frac{1}{1-D(t)} V_{in}(t)$ in CCM. $V_{in}(t)$ is the AC input voltage. The output bus voltage increases with the increasing duty cycle.

In the three-phase AC grid condition, with connected nodes *A*, *B* and *C* to the input terminals of the three-phase AC grid, respectively, and opened the relay between nodes *A* and *B*, the AC/DC stage changes to three-phase full-bridge topology with fixed frequency Space Vector PWM (SVPWM) control.

For both single-phase and three-phase operations, the AC/DC stage control mainly consisted of a phase lock loop (PLL), outer-loop voltage regulator and inter-loop current regulator. The PLL was responsible for locking and generating sinewave reference for the use of the current reference signal, which was in phase with the single-phase/ three-phase AC grid voltages. The outer-loop voltage regulator was responsible for regulating the bus voltage. The current regulator was responsible for controlling the input single-phase and three-phase input current sinusoidally with as small as possible reactive current content.

B. DC/DC stage design

The DC/DC stage is a bidirectional isolated DC-DC *CLLLC* Dual Active Bridge (DAB) converter with a variable DC-Link voltage input from the PFC and a battery-terminal output, which includes the following elements. Eight power switches S_7-S_{14} are high-frequency SiC MOSFETs, forming two identical H-bridges separated by a high-frequency transformer with a symmetric *CLLLC* resonant network, which is capable of bidirectional operation with its phase-shift modulation for both battery-charging mode and discharging mode.

For phase shift modulation of the DAB converter, four switch pairs are controlled to commutate complementarily at a fixed switching frequency f_s with a fixed duty cycle of 0.5. By introducing an internal phase shift, α_p, between S_7/S_8 and S_9/S_{10}, a high-frequency pulse width-modulated three-level AC voltage v_p ($+V_{bus}$, 0, $-V_{bus}$) with a variable duty ratio is generated at the primary-side H-bridge as α_p varies between 0 and 180°. Similarly, a second three-level ac voltage v_s ($+V_{bat}$, 0, $-V_{bat}$) is generated at the secondary-side H-bridge by introducing an internal phase shift α_s between S_{11}/S_{12} and S_{13}/S_{14}. For transferring power between V_{bus} and V_{bat}, v_s is phase shifted from v_p by an external phase shift θ, where θ is defined to be positive when v_s leads v_p and power is transferred from V_{bus} to V_{bat}, and vice versa.

For battery charging mode, the converter is designed to modulate α_p, α_s, and θ to achieve the required output voltage or current. α_p and α_s varies from 0˚ to 180˚ and θ varies from 0˚ to 90˚. As the battery voltage varies widely from 240V to 500V, an Adaptive Power Control (APC) is also implemented, the detail of which will be discussed in the next section, so that a variable bus voltage from the PFC converter is designed to minimize reactive power in the both-side bridges and achieve higher efficiency for both single-phase and three-phase operation across the battery voltage range.

The bus voltage varies from 390V to 500V for single-phase operation and from 580V to 700V for three-phase operation. In battery discharging mode, the *CLLLC* DAB converter is designed to regular the bus voltage according to battery voltage and output power. Similar to the charging mode, α_p and α_s vary from 0˚ to 180˚, but θ varies from 0˚ to -90˚ to realize the reverse power flow. Meanwhile, the bidirectional PFC converter operates in single-phase and three-phase inverter modes.

To examine the power transfer of the *CLLLC* DAB converter for both battery charging and discharging modes, First Harmonic Analysis (FHA) is applied to simplify the model of the *CLLLC* DAB converter. The diagrams of the FHA model and further simplified model with parameters referred to the primary side are shown in fig. 2.

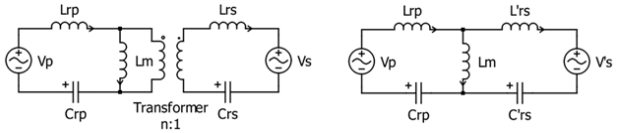

(a) (b)

Fig. 2. (a) FHA model of *CLLLC* DAB converter and (b) simplified model with parameters referred to the primary side

The parameters of the *CLLLC* DAB converter are as follows:

V_{bus}	Bus voltage	C_{rp}	Primary-side resonant capacitor
V_{bat}	Battery voltage	L_m	Magnetizing inductor
V_p	Primary voltage	L_{rs}	Secondary-side resonant inductor
V_s	Secondary voltage	α_p	Primary-side duty ratio
n	Turns ratio of the transformer	α_s	Secondary-side duty ratio
L_{rp}	Primary-side resonant inductor	θ	Phase shift between primary and secondary sides

From the FHA model, the duty-modulated fundamental tank voltages can be represented by

$$V_p = |V_p| \angle 0° = \frac{4}{\pi\sqrt{2}} V_{bus} \sin\frac{\alpha_p}{2} \quad (1)$$

$$V_s = |V_s| \angle \theta = \frac{4}{\pi\sqrt{2}} V_{bat} \sin\frac{\alpha_s}{2} (\cos\theta + j \sin\theta) \quad (2)$$

The *CLLLC* is tuned at the resonance point.

$$Z_{rp} = Z'_{rs} = -Z_m \quad (3)$$

where $Z_{rp} = sL_{rp} + \frac{1}{sC_{rp}}, Z'_{rs} = sL'_{rs} + \frac{1}{sC'_{rs}}, Z_m = sL_m, L'_{rs} = n^2 L_{rs}, C'_{rs} = \frac{C_{rs}}{n^2}$

Therefore, the fundamental tank currents magnitude can be represented by

$$I_p = |I_p| \angle \theta - 90° = \frac{1}{|Z_m|} \frac{4}{\pi\sqrt{2}} V_{bat} \sin\frac{\alpha_s}{2} [\cos(\theta - 90°) + j \sin(\theta - 90°)] \quad (4)$$

$$I_s = |I_s|\angle 90° = \frac{1}{|Z_m|}\frac{4}{\pi\sqrt{2}} nV_{bus} \sin\frac{\alpha_p}{2}[\cos 90° + j\sin 90°] \quad (5)$$

The power transfer can be calculated by evaluating the real product of V_p and I_p.

$$P = Re[V_p I_p] = \frac{8nV_{bus}V_{bat}}{\pi^2|Z_m|} \times M \quad (6)$$

where $M = \sin\frac{\alpha_p}{2}\sin\frac{\alpha_s}{2}\sin\theta$

θ is the phase shift angle between the primary and secondary sides, $0° \le \theta \le 90°$ for charging mode and $-90° \le \theta \le 0°$ for discharge mode.
The output battery current can be further calculated by (7).

$$I_{bat} = \frac{P}{V_{bat}} = \frac{8nV_{bus}}{\pi^2|Z_m|} M \quad (7)$$

In charging operation, α_p and α_s are identical and equal to α; meanwhile, θ is set to 0.45α to ensure Zero Voltage Switching (ZVS) conditions for both primary and secondary sides MOSFETs. Similarly, in discharging operation, θ is set to -0.45α to achieve ZVS for all the MOSFETs.

The maximum modulation M_{max} factor equals to $\sin^2\left(\frac{180°}{2}\right)\sin(0.45 \times 180°) = \sin 81°$. It is noted that the ZVS condition is independent of the power levels and input-to-output voltage ratio, which greatly simplifies its practical realization.

C. Adaptive power control design

An APC was derived and the routine is shown in fig. 3. It was implemented in the firmware of the PFC and DAB digital controllers to control the output of the proposed OBC. In the beginning, preset constants are given, including maximum battery current limit I_{bat_max}, maximum and minimum bus voltage limits V_{bus_min} and V_{bus_max}, and reference output power P_{ref}. Three variables are measured, including the battery voltage V_{bat}, current I_{bat} and the bus voltage V_{bus}. The battery reference current I_{bat_ref} is calculated as P_{ref}/V_{bat}. When computed I_{bat_ref} is less than or equal to the battery current limit I_{bat_max}, then Constant Power (CP) mode is used; otherwise, then Constant Current (CC) mode is used, and I_{bat_ref} is reduced to I_{bat_max}. V_{bus_ref} is calculated as KI_{bat_ref}, where I_{bat_ref} was limited to I_{bat_max} for CC mode or is P_{ref}/V_{bat} for CP mode. When the calculated V_{bus_ref} is greater than the V_{bus_max}, then V_{bus_ref} is reduced to V_{bus_max}, and charging uses CC mode. When the calculated V_{bus_ref} is less than V_{bus_min}, then V_{bus_ref} is raised to V_{bus_min} in either CP or CC mode. The measured V_{bus} is compared to the calculated V_{bus_ref} to adjust the duty cycle of the PWM control signals generated by the PFC digital controller to the MOSFETs in AC/DC stage. I_{bat} is compared to I_{bat_ref} for CP or CC mode, or V_{bat} is compared to V_{bat_max} for CV mode, to adjust the duty cycle ratio and phase shift between the primary and secondary PSM control signals that are generated by DAB digital controller to primary-side and secondary-side MOSFETs in DC/DC stage. After that, new measurements of V_{bus}, I_{bat}, or V_{bat} are taken, and the above-mentioned steps repeat again.

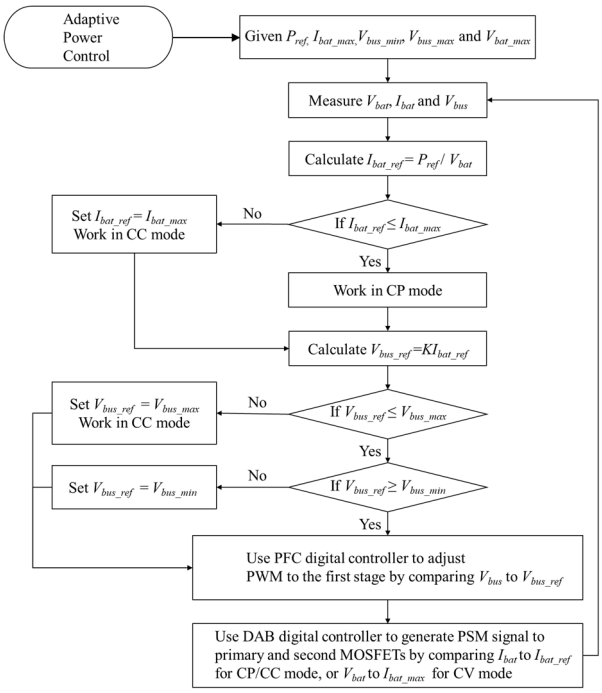

Fig. 3. Flowchart of the proposed APC

The main objective of active power control is to keep the modulation factor M as high as possible so that the circulating current in the both-side bridges of the *CLLLC* DAB converter can be minimized. Assume that there is a +/-10% change in I_{bat} due to the variation in other parameters. $V_{bus,ref}$ is set to a function of the battery reference current $I_{bat,ref}$ in CP mode. The battery reference current $I_{bat,ref}$ is calculated as P_{ref}/V_{bat} when $I_{bat,ref}$ is less than or equal to the battery current limit $I_{bat,max}$ for constant power charging mode.

$$V_{bus,ref} = \frac{1}{0.9}\frac{\pi^2|Z_m|}{8nM_{max}} I_{bat,ref} = KI_{bat,ref} \quad (8)$$

where $K = \frac{1}{0.9}\frac{\pi^2|Z_m|}{8nM_{max}}$, and it is a constant and dependent on the designed parameter of the *CLLLC* converter.

D. Mechanical design

The proposed power module was designed with a liquid cooling solution with a liquid-cooled base plate integrated with copper tubes for liquid circulation. The power semiconductors on the power board, magnetic components of the resonant tank, and PFC chokes are installed directly on the base plate. Those are the main heat sources of the power module, and they can be effectively cooled by the base plate during operations. Fig. 4 shows the installation and mechanical fixation of the V2G bidirectional OBC prototype.

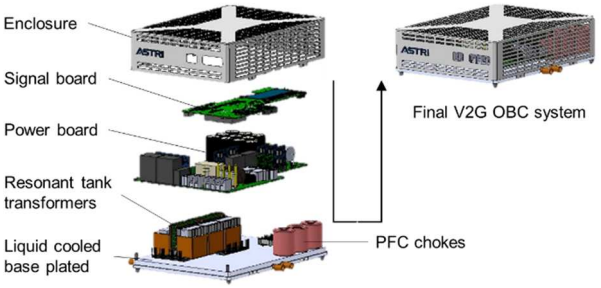

Fig. 4. Installation of the proposed V2G bidirectional OBC prototype

III. Experimental Verifications

Table. I Key electrical specifications

Item	Single-phase	Three-phase	Unit
Line voltage	220	380	V
Line frequency	50	50	Hz
Rated power	6.6	11	kW
Battery voltage	240 – 500		V
Maximum efficiency	96.5		%
Power density	1.54		kW/L
Cooling	Liquid cool		
Isolation	High-frequency transformer		

A prototype of the proposed OBC was designed and built with key electrical specifications, as shown in Table. I. Fig. 5(a) shows the system integration of the proposed OBC. The dimensions are 245mm (W) x 339mm (L) x 86mm (H), and the power density is 1.54kW/L. Fig. 5(b) shows the individual PCBA of the proposed OBC, including the power board and control board. The power board contains both AC/DC and DC/DC stages except for magnetics components. The "Power board (top side)" figure shows the gate driver boards of the MOSFETs that are vertically installed to the power board for better space utilization. The "Power board (bottom side)" figure shows the power semiconductors are mounted on the bottom side of the board, which finally attach to the liquid-cooled base plate for cooling. The integration of power and control boards is shown in the "Power board and control board integration" figure. The control board is installed on top of the power board with standoffs in between. A TI 28379D DSP control card is used to perform the digital control of the proposed OBC. The "Power flow" figure shows the directions of power flows between the AC grid and battery terminals. The one with red arrows shows the charging mode operation, while the one with blue arrows shows discharging mode operation. There is no crossing in current / power flow between the AC/DC and DC/DC stages which reduced interference and noise, particularly the interference via PCB.

Fig. 6 shows the test setup of the proposed OBC for both three-phase and single-phase operations. The AC terminal of the prototype is connected to a regenerative AC grid simulator. Meanwhile, the DC terminal of the prototype is connected to an E-load and in parallel with a power supply to simulate a battery. The OBC performs charging in the three-phase operation and charging/discharging in the

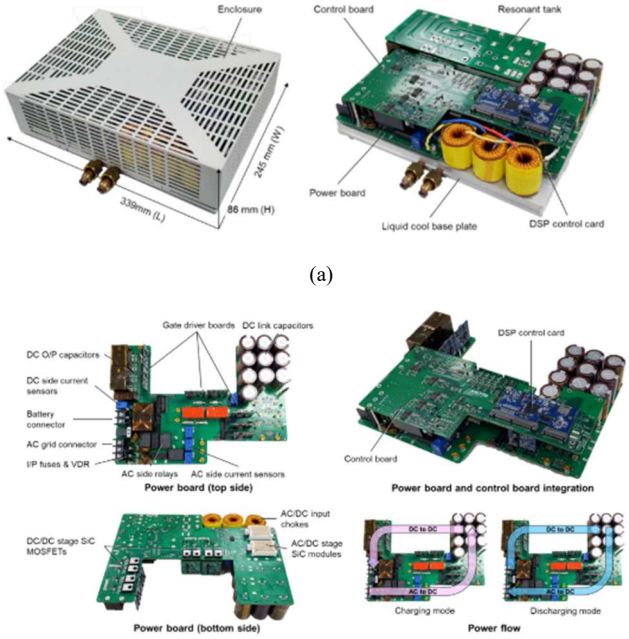

Fig. 5. Prototype of the proposed OBC: (a) the full system integration and (b) individual PCBA, including the power board and control board.

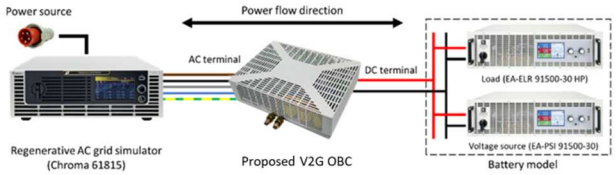

Fig. 6 Test setup of the proposed V2G bidirectional OBC

single-phase operation. In the following section, the electrical test results of the proposed OBC will be reported.

A. Single-phase charging operation

In the single-phase operation, the AC/DC stage of the proposed OBC worked as a two-phase interleaved totem-pole topology with fixed frequency CCM control; the DC/DC stage worked as *CLLLC* DAB topology with fixed frequency and variable phase shift control. Fig. 7 shows the measured single-phase steady state CC mode and CP mode operation waveforms, including AC grid voltage, grid current, bus voltage and output current on the top waveform, bridge voltages and bridge currents of DC/DC stage on the bottom waveform. Figs. 6 (a) and (b) refer to the 18A CC mode operation for battery voltage at 240V and 6.6kW CP mode for battery voltage at 500V, respectively.

B. Three-phase charging operation

In the three-phase operation, the AC/DC stage of the proposed OBC was reconfigured and worked as a three-phase full-bridge topology with fixed frequency continuous SVPWM control. Same as the single-phase operation, the DC/DC stage worked as *CLLLC* DAB topology with variable phase shift control, but its bus voltage was higher. Fig. 8 shows the measured three-phase steady state CC mode and CP mode operation waveforms, including AC line-line voltage, grid current on the top

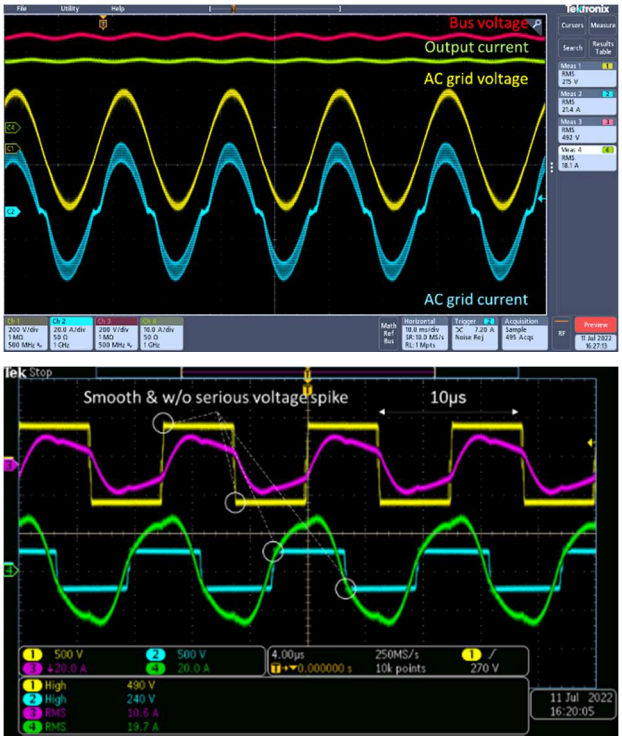

(a)

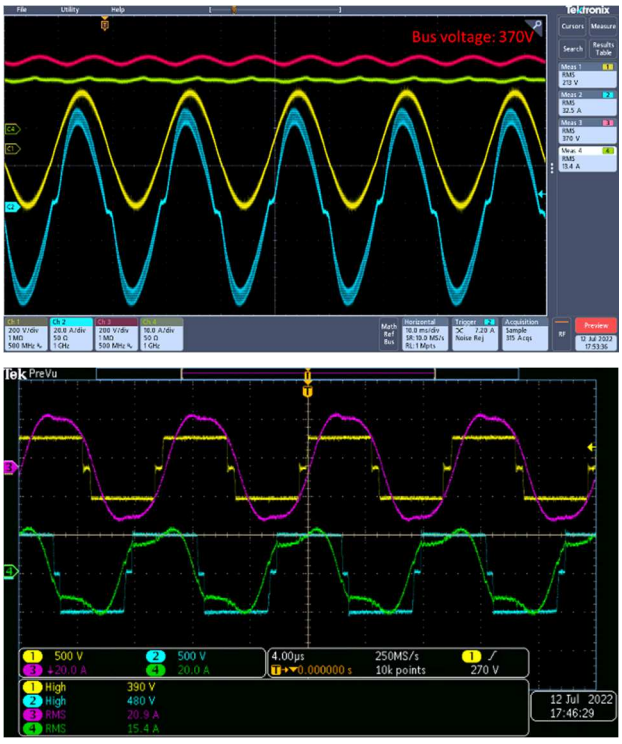

(b)

Fig. 7. Steady-state waveforms of single-phase charging (a) at 18A constant output current for battery voltage at 240V and (b) at 6.6kW constant power for battery voltage at 500V

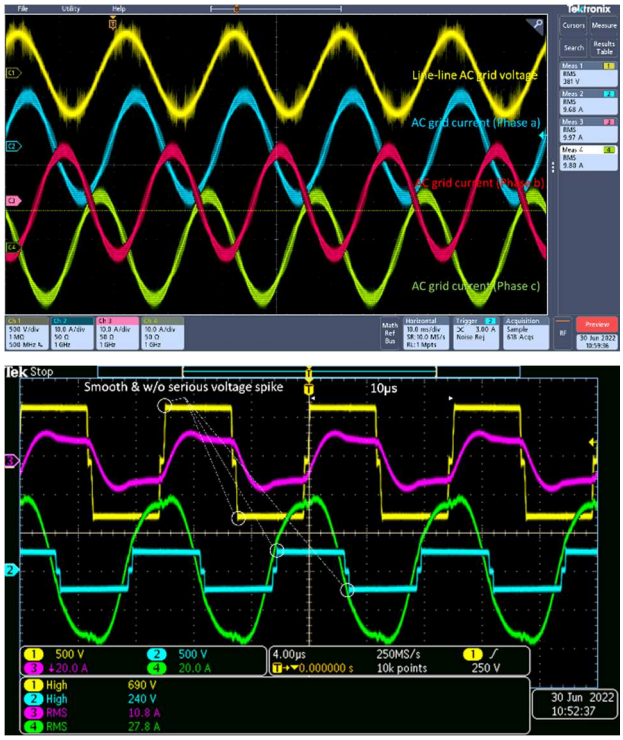

(a)

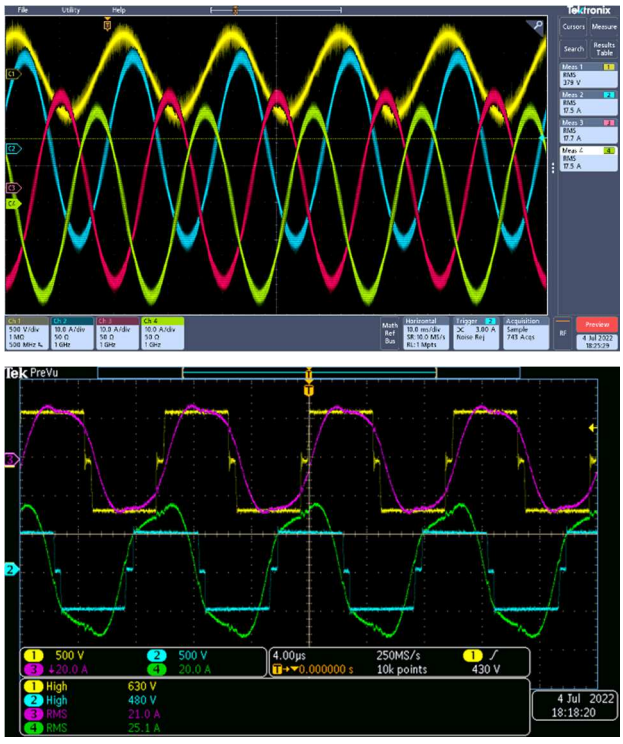

(b)

Fig. 8. Steady-state waveforms of three-phase charging at (a) 25A CC mode for battery voltage at 240V battery voltage and (b) at 11kW CP mode for 500V battery voltage

waveform, bridge voltages and bridge currents of the DC/DC stage on the bottom waveform. Figs. 7 (a) and (b) refer to the 25A CC mode operation for battery voltage at 240V and 11kW CP mode for battery voltage at 500V, respectively.

C. Single-phase discharging operation

In single-phase CP discharge mode, the output AC terminal was connected to a regenerative grid simulator to model the situation of on-grid operation, i.e., the proposed OBC discharged power to the grid. Fig. 9 shows the AC output voltage, AC output current, bus voltage and battery

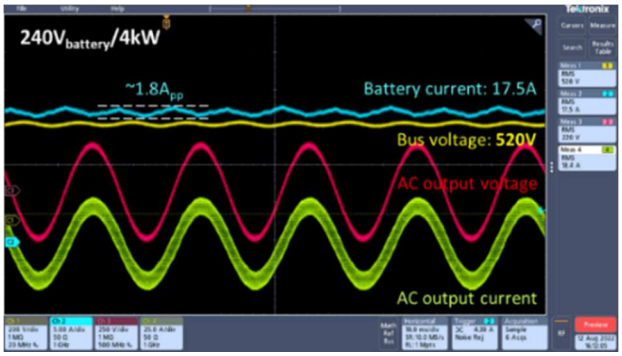

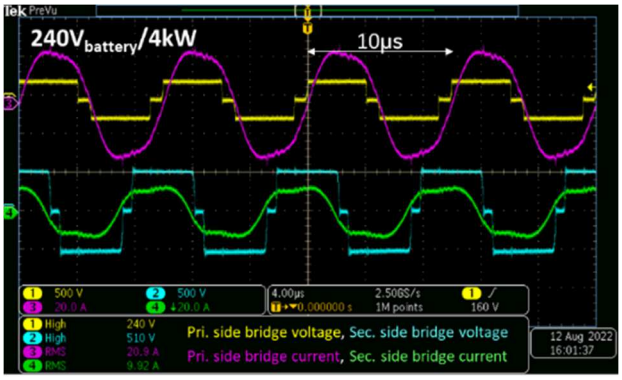

(a)

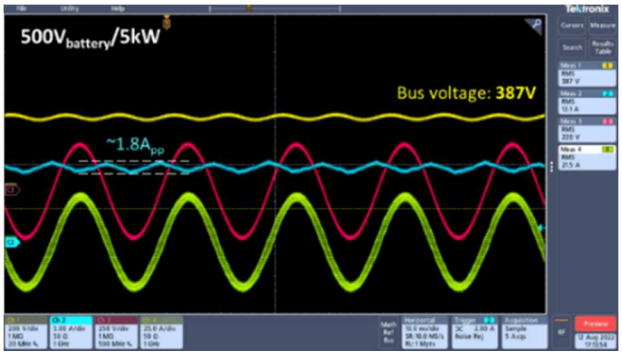

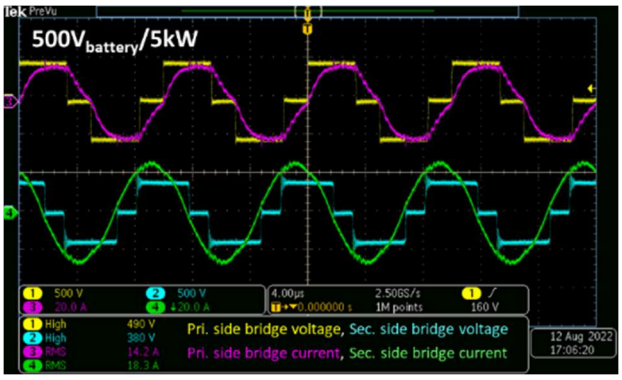

(b)

Fig. 9. Steady-state waveforms of single-phase discharging (a) at 4kW constant output power for battery voltage at 240V and (b) at 5kW constant power for battery voltage at 500V

current on the waveform. Very little voltage or current spike occurred during switching transients. Fig. 8 (a)-(b) refers to the 4kW CP mode operation for battery voltage at 240V and 5kW CP mode for battery voltage at 500V, respectively. With the APC, bus voltage was regulated and varied from 380V to 520V as a function of rated power and battery voltage. For battery voltage above 300V, the rated power was maintained at 5kW. The rated power was reduced from 5kW to 4kW for battery voltage decreased from 300V to 240V due to the limit of maximum battery current. Under a double-loop control of the DAB stage, an outer voltage control loop and an inner current control loop, the input battery current was maintained at a reasonably stable DC format. It was immunized from the influence of the double-line frequency component. It implied that the proposed OBC was a battery-friendly system which would not affect the battery life caused by current ripple.

D. Start-up & turn-off operation

Figs. 9 and 10 show start-up and turn-off waveforms at three-phase 11kW output power and 500V battery voltage. As shown in Fig. 10 Start-up (AC/DC), the input current gradually increased as the bus voltage was ramped from 538 to 580V; the DAB stage started the soft-start process, and the output current started to ramp to the target level. When the output current reached the target level, the proposed OBC operated in a steady state, and the bus voltage reference was adjusted automatically by APC with respect to the actual battery voltage level during the charging period. The Start-up (DC/DC) waveforms show the primary and secondary sides resonant tank switching voltage and current waveforms. The resonant tank currents and red and green waveforms were increased gradually during start-up. Fig. 11 shows the turn-off waveforms of AC/DC and DC/DC stages. The switching voltage and current waveforms were reduced to zero without any over-shoot of both AC/DC and DC/DC stages. It was concluded that the OBC could start up and turn off smoothly at full load conditions.

E. Efficiency measurement

Fig 11 shows the measured efficiency for single-phase charging, three-phase charging and single-phase discharging at different battery voltages and load levels. In the single-phase charging mode, the efficiency reached 96.54% at 240V battery voltage and 3.3kW load power condition, as shown in Fig. 12(a). The dash lines indicate the peak efficiency curves at single-phase CP modes charging. The proposed OBC can adjust the charging current/power to give a very efficient charging process at single-phase with efficiencies between 96.54% and 95.73% from 240V to 500V battery voltage. In three-phase charging mode, the proposed OBC reached an efficiency of 96.44% at 450V battery voltage and 9kW load power condition, as shown in Fig. 12(b). Similar to the single-phase charging mode, the dash lines indicate the peak efficiency at the three-phase CP charging mode. The proposed OBC can adjust the charging current/power along the battery voltage to give a very efficient charging process at three-phase with efficiency between 96.14%

and 96.46% from 240V to 500V battery voltage.

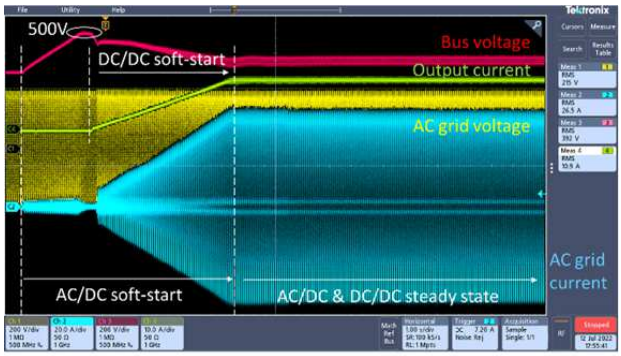

Start-up (AC/DC)

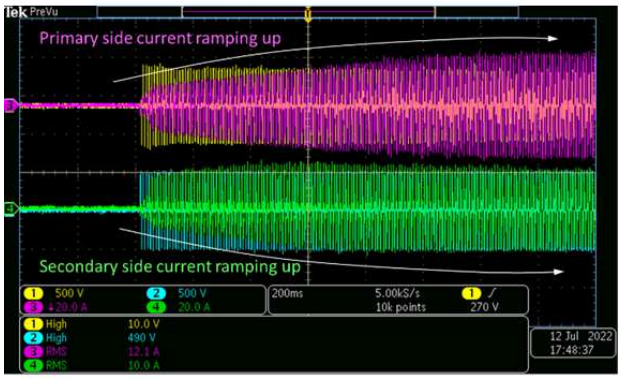

Start-up (DC/DC stage)

Fig. 10. Start-up waveforms at three-phase, 11kW, 500V battery voltage

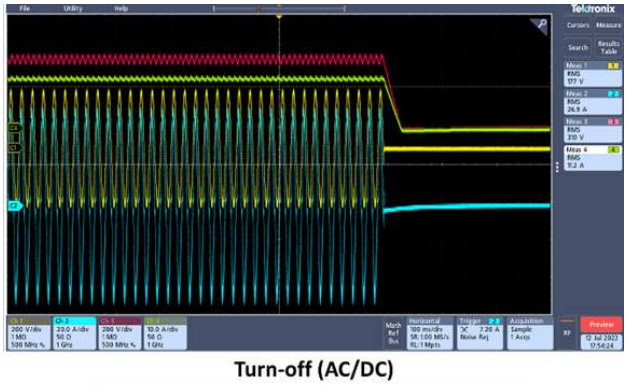

Turn-off (AC/DC)

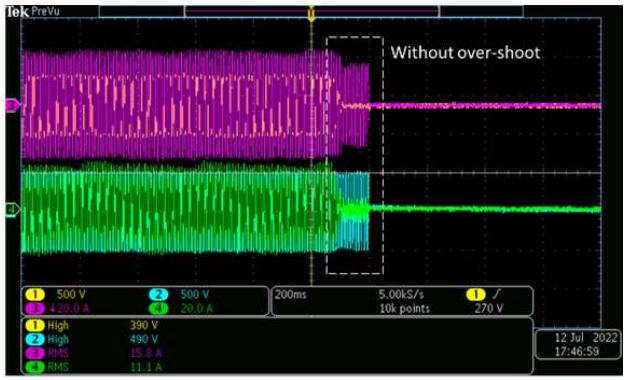

Turn-off (DC/DC stage)

Fig. 11. Turn-off waveforms at three-phase, 11kW, 500V battery voltage

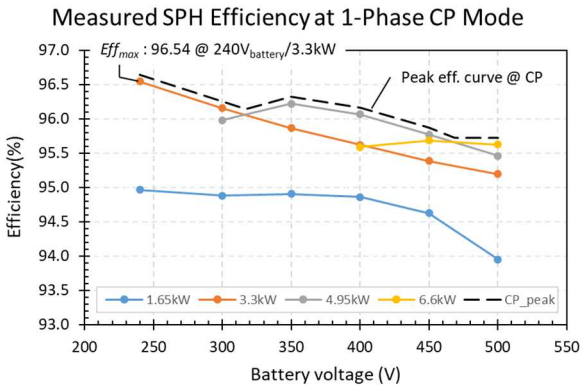

(a)

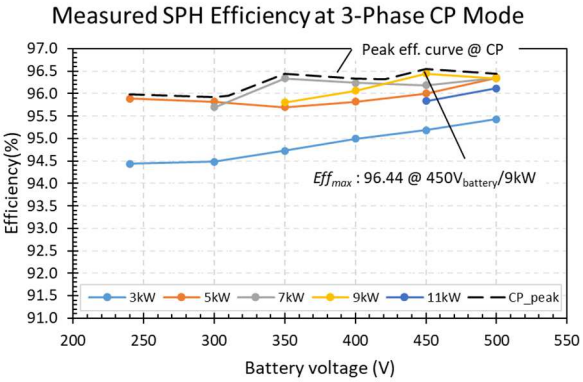

(b)

Fig. 12. The measured efficiency of the proposed OBC at (a) single-phase charging mode, (b) three-phase charging mode.

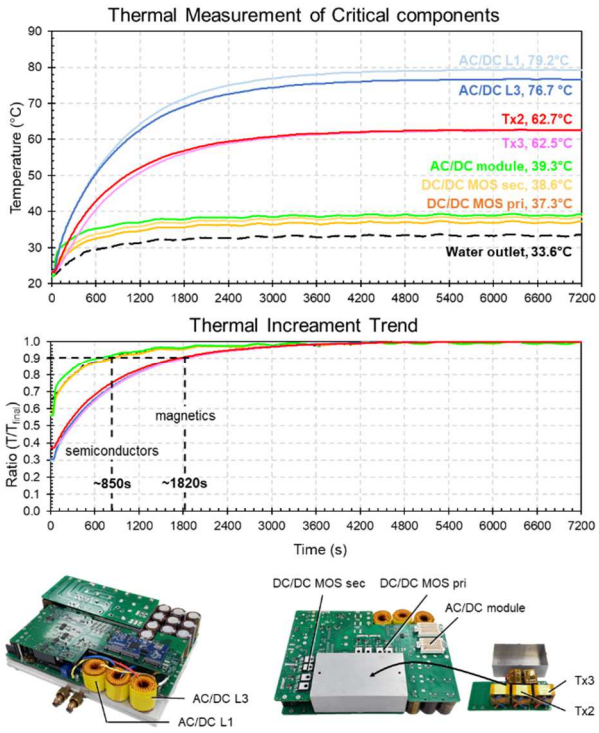

Fig. 13.Thermal measurement results of critical components at 11kW and 500V battery voltage

The temperature distribution of the critical components under three-phase 11kW and 500V battery voltage operation was conducted with an initial water temperature of 22.1°C. Results are shown in fig. 13. The top figure shows the measured actual temperature of the components and the second figure shows the time to thermal equbilium. The liquid temperature at the base plate liquid outlet was increased from 11.5°C to 33.6°C. The hottest component was the AC/DC inductor 1, and it reached 79.2°C with an increment of 55.8°C. The limit of wire insolation material is 130°C, and the limits of core material for AC/DC inductor and DC/DC transformer are 200°C and 220°C, respectively. Therefore, there is ~120°C thermal margin for the magnetic parts. Semiconductors were effectively cooled by the liquid-cooled base plate. The case temperature of the MOSFET was below 40°C. It shows the cooling design is very effective for the V2G bidirectional OBC prototype.

IV. Conclusions

A single-phase and three-phase grids compatible V2G EV on-board bidirectional charger was developed. With the proposed power stage structure and control method, the on-board charger is compatible with the single-phase 6.6kW and three-phase 11kW AC voltage and battery voltage from 240V to 500V. The operating principle and experimental verification for different operation modes, including charging/discharging and single-phase/three-phase AC input, have been explained and implemented successfully. Moreover, an Adaptive Power Control (APC) methodology for 2-stage power conversion has been developed and implemented so that the power efficiency of the charger reached 96.54%.

Acknowledgement

We acknowledge financial support and valuable advice from Hong Kong Innovation and Technology Commission. (Project no. ART/302CP)

References

[1]. A. Khaligh and M. D'Antonio, "Global Trends in High-Power On-Board Chargers for Electric Vehicles," in *IEEE Transactions on Vehicular Technology*, vol. 68, no. 4, pp. 3306-3324, April 2019, doi: 10.1109/TVT.2019.2897050.

[2]. Global EV Outlook 2021, International Energy Agency, April 2021. Available at: https://www.iea.org/reports/global-ev-outlook-2021.

[3]. Hong Kong Roadmap on Popularisation of Electric Vehicles, Environment Bureau, Hong Kong Government, March 2021. Available at: https://www.evhomecharging.gov.hk/downloads/ev_booklet_en.pdf

[4]. J. Yuan, L. Dorn-Gomba, A. D. Callegaro, J. Reimers and A. Emadi, "A Review of Bidirectional On-Board Chargers for Electric Vehicles," in *IEEE Access*, vol. 9, pp. 51501-51518, 2021, doi: 10.1109/ACCESS.2021.3069448.

[5]. S. Semsar, T. Soong and P. W. Lehn, "On-Board Single-Phase Integrated Electric Vehicle Charger With V2G Functionality," in *IEEE Transactions on Power Electronics*, vol. 35, no. 11, pp. 12072-12084, Nov. 2020, doi: 10.1109/TPEL.2020.2982326.

[6]. W. L. Malan, D. M. Vilathgamuwa and G. R. Walker, "Modeling and Control of a Resonant Dual Active Bridge With a Tuned CLLC Network," in *IEEE Transactions on Power Electronics*, vol. 31, no. 10, pp. 7297-7310, Oct. 2016, doi: 10.1109/TPEL.2015.2507787.